Cement & Concrete Composites 37 (2013) 241–245

Contents lists available at SciVerse ScienceDirect

Cement & Concrete Composites

journal homepage: www.elsevier.com/locate/cemconcomp

# Spatially resolved investigation of complex multi-phase systems using μXRF, SEM-EDX and high resolution SyXRD

Moritz Caspar Schlegel [a], Urs Mueller [a], Katarina Malaga [c], Ulrich Panne [a,b], Franziska Emmerling [a,*]

[a] BAM Federal Institute for Materials Research and Testing, Richard-Willstätter-Str. 11, 12489 Berlin, Germany
[b] Department of Chemistry, Humboldt University zu Berlin, Brook-Taylor-Str. 2, 12489 Berlin, Germany
[c] CBI Swedish Cement and Concrete Research Institute, Brinellgatan 4, 504 62 Borås, Sweden

ARTICLE INFO

*Article history:*
Received 16 January 2012
Received in revised form 12 August 2012
Accepted 18 August 2012
Available online 29 August 2012

*Keywords:*
EDX-SEM
SyXRD
Spatial investigations
Comparison
High resolution
Cement paste
Sulfate attack
Damaging mechanism

ABSTRACT

Spatially resolved analysis of complex multi-phase systems can be validated through different analytical methods. This study compares investigations by scanning electron microscopy coupled with energy dispersive X-ray fluorescence analysis and high resolution X-ray diffraction. The studied sulfate attacked cement paste containing fly ashes consists of different interacting crystalline and amorphous phases. The complementary methods revealed in detail changes in phase composition due to the chemical attack. The advantages and disadvantages of both methods are discussed and suggestions are given for combining them with additional methods to maximize the information content.



## 1. Introduction

Spatially resolved investigations using electron or X-ray radiation are often used to characterize complex multi-phase systems such as cement pastes [2,3,8,12–14,16,18,22,23]. The obtained spatial resolution differs strongly depending on the experimental method applied and ranges between several μm down to the nm-scale. Examples for application of an electron beam are reported by Richardson [20,21], who analyzed the microstructure of cement paste by transmission electron microscopy. An example for the application of spatially resolved X-ray diffraction analysis is described by Paris et al. [19]. This setup allows the phase analysis of the cement matrix in detail and the reconstruction of the change of the phase composition induced by chemical attacks [4].

The cement matrix mainly consisted of portlandite ($Ca(OH)_2$), monosulfate ($Ca_4Al_2(SO_4)(OH)_{12}\cdot 6H_2O$) and C–S–H, whereas the inner C–S–H phases are more influenced by the cement clinker. The sulfate solution penetrated the sample and induced, among the formation of gypsum, the crystallization of $Ca^{2+}$, $Al^{3+}$, and $SO_4^{2-}$ bearing secondary phases. These phases are part of two groups of phases, the alumina ferrite mono(sulfate) (AFm, $[Ca_2(Al,Fe)(OH)_6]\cdot x\cdot yH_2O$, $x = SO_4^{2-}$, $CO_3^{2-}$, $Cl^-$, $OH^-$) and alumina ferrite tri(sulfate) phases (AFt, $[Ca_3Al(OH)_6\ 12H_2O]_2\cdot x\cdot yH_2O$, $x = 3SO_4^{2-}$, $3CO_3^{2-}$) [1,7,9,10,15,17]. The phases replace the original microstructure and induce damaging processes such as volume expansion by the crystallization process of the AFt phases. The resulting crystallization pressure induces crack propagation which increases the penetration depth of the solution.

Our study compares results of investigations of complex multi phase systems by micro-X-ray fluorescence analysis (μXRF), scanning electron microscopy coupled with energy dispersive X-ray fluorescence analysis (SEM-EDX), and a high resolution X-ray diffraction method based on synchrotron radiation (SyXRD). A cement paste containing fly ash, a common supplementary cementitious material and mineral addition in concrete, was subjected to a sulfate attack. The samples represent a system consisting of interacting crystalline and amorphous phases. These complex multi phase systems were analyzed on the μm scale. The analyses were focused on reaction fronts moving from the outside to the inside of a cementitious material, changing its microstructure. Finally, both experimental methods were compared, focused on applicability.

## 2. Sample preparation

The samples were prepared with a w/c ratio of 0.50, a dimension of $40 \times 40 \times 160\ mm^3$ and consisted of ordinary portland ce-

* Corresponding author. Tel.: +49 30 8104 1133; fax: +49 30 8104 1139.
*E-mail address:* franziska.emmerling@bam.de (F. Emmerling).

0958-9465/$ - see front matter © 2012 Elsevier Ltd. All rights reserved.
http://dx.doi.org/10.1016/j.cemconcomp.2012.08.018

ment (OPC) with 30 wt.% of class F fly ash (Table 1). During the hardening process, the samples were stored above water over a time period of 28 d. Afterwards, the sulfate attack was simulated under laboratory conditions by embedding the sample in an aqueous solution with a high concentration of $Na_2SO_4$ (30 g/L) over a time period of 6 months. After the exposure the samples were embedded in epoxy resin, cut and polished into thick sections with a dimension of 20 × 40 × 0.2 mm. During the preparation process, the samples were cooled with petroleum to avoid dissolution of water soluble phases.

## 3. Experimental methods

The distribution of sulfate ions within the cement paste samples were localized by elemental mapping using μXRF (Eagle III, EDAX, Röntgenanalytik Systeme GmbH & Co. KG, Wiesbaden, Germany) operating at 40 kV and 120 mA with a spatial resolution of 40 μm. The measurements were performed on areas of 15 × 20 $mm^2$ and illustrated the progress of sulfate ingress at a given time. The information gained by this method consisted in high resolution concentration profiles of sulfur (representing sulfate) and other elements such as Ca, Fe, or Si. This enables localizing of the secondary phases. The identification of the secondary phases by SEM-EDX and SyXRD focused on crucial changes in the sulfur profile.

The SEM (Joel, JSM-5310LV, Sollentuna, Sweden)-EDX (Oxford, Stockholm, Sweden) was operated with 15 kV and 33 μA in the backscatter electron mode. 100–140 spectra were collected from each area of different sulfur concentrations localized by the μXRF. The spot size and acquisition time was 2 μm and 30 s. The already hydrated cement matrix was measured, which contains secondary phases crystallized during the sulfate attack. The matrix mainly consisted of C–S–H phases, portlandite and monosulfate. The distribution of these three phases did not influence the results and corresponding counting statistics. Analyzing the hydrated matrix prevents interferences of the cement clinker phase and inner product C–S–H forms on the collected data. Finally, the elemental concentrations were normalized by Ca. A frequently applied measurement strategy for the determination of the phase composition was used. According to several authors, the method based on calculation and presentation of the ratios Al/Ca against Si/Ca respectively Al/Ca against S/Ca. In this study, the Al/Ca and S/Ca ratios of the pure C–S–H (Al/Ca = 0, S/Ca = 0), Monosulfate (Al/Ca = 0.5, S/Ca = 0.25), and the secondary phases such as ettringite (Al/Ca = 1/3, S/Ca = 0.5) and gypsum (Al/Ca = 0, S/Ca = 1) were used [5,6,11,24]. The data points of the above mentioned pure phases are connected with lines representing the ratios of different secondary phases within the cement matrix in the same area.

The spatial analyses by SyXRD were performed at the microfocus beamline μSpot (BESSY II of the Helmholtz Centre Berlin for Materials and Energy) in transmission geometry (see Fig. 1). The experiments were carried out with a wavelength of 0.8565 Å using a Si (1 1 1) double-crystal monochromator. The focusing system of the beamline provides a beam diameter of 10 μm at a photon flux of $1 \times 10^9$ $s^{-1}$ at a ring current of 200 mA with a horizontal and vertical divergence of less than 1 mrad [19]. The diffracted intensities were collected 210 mm behind the sample position with a two-dimensional MarMosaic CCD X-ray detector with 3072 × 3072 pixels. Profile scans were measured perpendicular to the sample surface and across the reaction fronts down to a profile depth of 3 mm. In order to improve sampling statistics the sample was continuously moved 10 mm parallel to the reaction front for 60 s during the profile scans. The resulting diffraction patterns were displayed in a top view to optimize the phase identification and to provide an overview of both reflections intensities and positions. The ocean data viewer software was used to combine the diffraction pattern and calculate the respective 3D-images (AWI, Bremen, Germany). The phase identification was orientated on the reflections positions and carried out with the search/match function of the EVA software (Bruker, Karlsruhe, Germany).

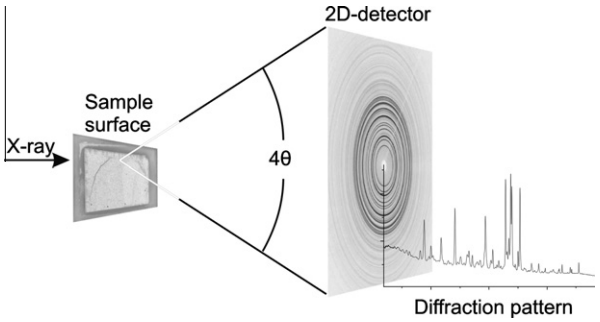


**Fig. 1.** Scheme of the experimental setup. X-rays penetrate the sample material and the diffracted intensities were detected with an area detector. The detector frames were integrated as a function of the center distance and the diffraction pattern were calculated.

## 4. Results

The results of the analysis by μXRF are displayed in Fig. 2. The elemental mapping of the sulfur intensity shows four zones in which the relative sulfur concentration differs from each other (II > III > IV > I). The first zone showed a medium sulfur concentration beginning at the sample surface down to the profile depth of 0.5 mm (I). This region is followed by a very high concentration between 0.5 and 1.2 mm depth (II). Below the latter zone, a higher concentrated zone could be observed down to a profile depth of 1.2 mm (III). The relative sulfur concentration was low in the zone IV and increased down to a profile depth of about 6.5 mm. Below this depth, the relative sulfur concentration did not change significantly.

The calcium distribution is also displayed in Fig. 2 and shows very low concentrations of calcium at the sample surface area. Nevertheless, the relative concentration increases with increasing profile depth, especially in the first zone. In zone II, the relative concentration decreases directly at the border between zone I and II. Below the border, the relative concentration increases again, however with a shallower slope. In zone IV, the relative concentrations exhibit no significant changes.

Following μXRF analysis, for each of the four zones the composition of the hydrate phases was determined by microchemical methods (SEM-EDX). Fig. 3 shows the atom ratios Al/Ca against S/Ca. The spectra collected in the zone from the surface down to a profile depth of 0.5 μm revealed medium sulfur concentrations (I). The main part of the data points are between the line of pure C–S–H phases and ettringite and between the line of C–S–H phases and monosulfate, although a few spectra show relatively high Al

**Table 1**
Chemical composition of the ordinary Portland cement (wt.%).

| $SiO_2$ | $Al_2O_3$ | $Fe_2O_3$ | $Mn_2O_3$ | $TiO_2$ | CaO | MgO | $Na_2O$ | $K_2O$ | $Na_2O_{equi}$ | $SO_3$ | $Cl^-$ |
|---|---|---|---|---|---|---|---|---|---|---|---|
| 21.07 | 4.47 | 2.33 | 0.03 | 0.20 | 64.34 | 2.19 | 0.29 | 0.97 | 0.93 | 3.53 | 0.08 |

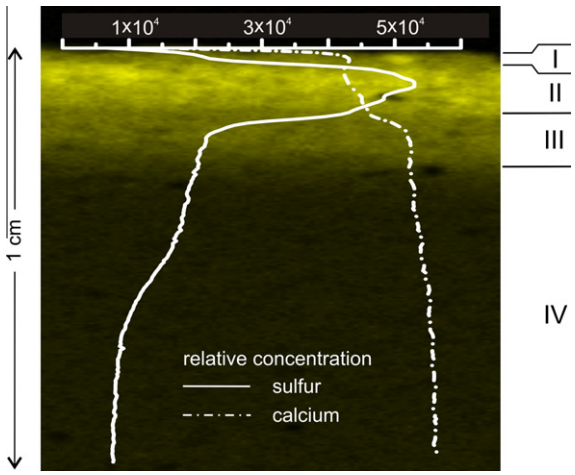


**Fig. 2.** Color-coded sulfur concentration from the sample surface down to a profile depth of 1 cm. Four zones (I–IV) with different concentrations are identified. The graph (white lines) represents the relative calcium and sulfur distribution as function of the profile depth.

concentrations probably due to the fly ash. The spectra collected in the zone below 0.5 μm show higher S/Ca atom ratios (II). The major part of the data points lies on the line between the pure C–S–H phases and ettringite and some data points are near the line between ettringite and gypsum. Below the area with the very high sulfur concentrations the spectra look similar to those collected at the sample surface area (III). The major part of the collected data points are on the line between the pure C–S–H phases and ettringite and on the line between the C–S–H phases and monosulfate. A few spectra show high Al concentrations probably through the fly ashes. All spectra collected in a profile depth of >2.7 mm exhibit low sulfur and high alumina concentration (IV). The data points lie on the line between the pure C–S–H phases and monosulfate.

The collected diffraction pattern received from high resolution SyXRD shows zoning effects similar to the results from the μXRF (see Fig. 4). The reflection positions change clearly at defined profile depths. For the area from the sample surface down to a profile depth of 0.5 mm, the phase identification based on the reflection positions shows a small amount of secondary ettringite. For the very high concentrated area from 0.5 to 1.2 mm, the amount of ettringite increases over the whole $2\theta$ range and gypsum was identified. For the high concentrated area from 1.2 to 2.7 mm as well as for the low concentrated zone, low amounts of ettringite and the absence of gypsum are found. The reflections intensities of ettringite decrease as a function of the profile depth and an AFm solid solution was identified down to profile depth of 2.25 mm.

## 5. Discussion

The μXRF analysis offers general information about the interactions of the sample material with the surrounded solution. The medium concentrated zone I represent a leaching zone, identified by the low Ca concentrations. The very high concentrated zone II represents the profile depths where the secondary phases already crystallized. The higher concentrated zone III represents the penetrations depth of the sulfate solution and the low concentrated zone IV the intact bulk. After localizing the different zones, the SEM-EDX and SyXRD analysis can be performed more focused on the crucial change of the phase composition.

The study performed by SEM-EDX provided valuable information on the change of the phase composition of the OPC with

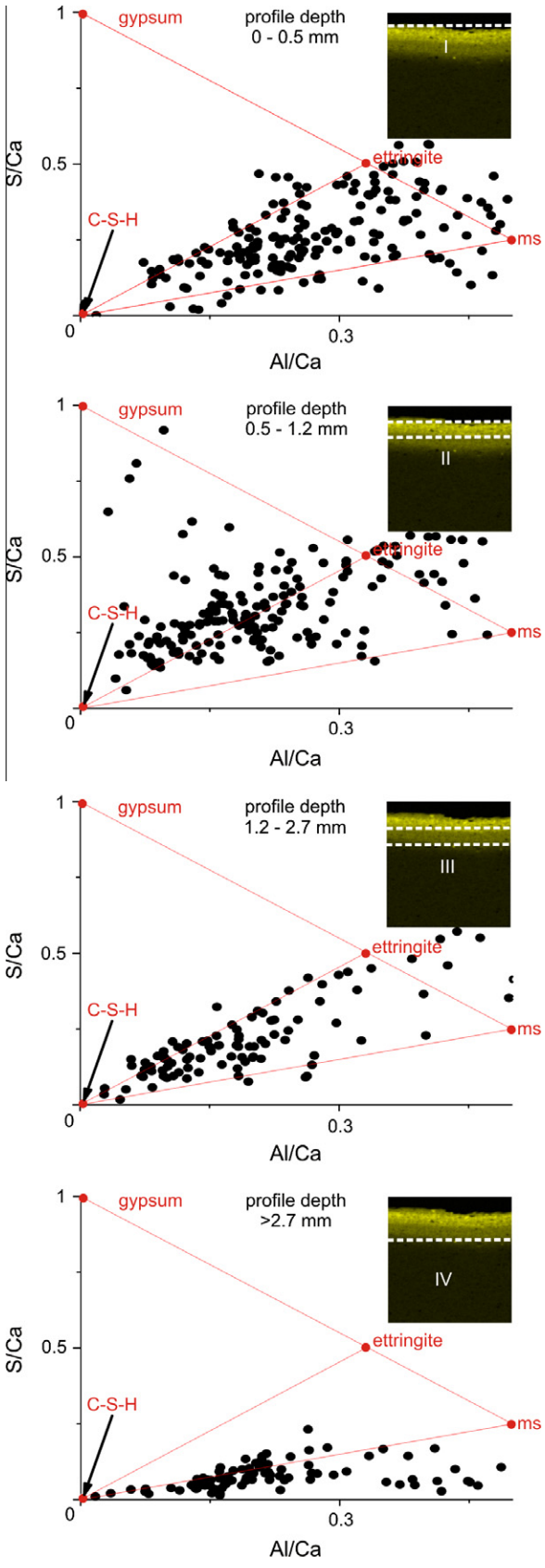


**Fig. 3.** S/Ca and Al/Ca ratios, estimated by SEM-EDX analysis. The ratios of the AFm end member monosulfate (ms), AFt end member Ettringite, gypsum and C–S–H phases are connected by red lines. (For interpretation of the references to color in this figure legend, the reader is referred to the web version of this article.)

30 wt.% of fly ash due to the sulfate attack. Different secondary phases were identified by calculating the Al/Ca and S/Ca atom ratios and visualizing the data. In this way, the interaction of the sulfate solution with the cementitious material can be characterized by using an experimental setup on the laboratory scale. Unfortunately, the measurement points have to be selected by the user manually to avoid spectra collected in partially hydrated clinker phases. This procedure is time consuming in relation to the acquisition time of the detector system. The measurement time depends on an acceptable counting statistics. Additionally, elemental mapping is essential, e.g. by μXRF, before investigating the sample material by SEM-EDX. Without any information about the profile depths of the areas with similar concentration, the whole region of interest has to be scanned. This increases the measurement time from minutes up to several hours or even days, which limits the application of this method.

Gollop and Taylor [11] suggested mapping a complete region of interest automatically and accepting only spectra with relative intensities between 70% and 80% of the maximum intensity. If the major amount of clinker phases is not already hydrated, a lot of measurements cannot be taken into consideration, which increases the measurement time as well.

The profile depths estimated by SyXRD, where the phase composition changes due to the sulfate attack, matched the profile depth localized by μXRF however more precisely (see Fig. 4). Compared to previous studies, the high spatial resolution obtained here offers a deep insight into the crystallization process of the secondary phases. As expected, the secondary sulfate phases ettringite and gypsum were identified, however in different profile depths. Ettringite crystallized over the whole analyzed profile depth and gypsum 0.5 mm the below the sample surface area. The formation of ettringite depends on the sulfate ingress itself. Obviously, the crystallization of gypsum is based on a local increase of the sulfate concentration. The investigations of the phase composition by high resolution SyXRD are independent of previous spatial chemical analysis. The measurements can be performed in an automatic scanning mode because the intensity of the crystalline secondary phases and the clinker phases can be separated. A measurement time of about 1 h/mm provides acceptable counting statistics. The spatial resolution is high enough to recognize sharp changes of the phase composition at defined profile depths. The collected data provides a detailed view into the changes of the crystalline phase composition. However, very high energies are necessary to penetrate the sample material, which is only available at synchrotron facilities.

This experimental approach is neither fixed nor developed exclusively for the investigations of cementitious materials. It can be used to perform investigations of many other multi-phase systems where crystalline phases interact with complex fluids, such as water/rock interactions.

Both the SEM-EDX and SyXRD are suitable to obtain a deep inside into the change of the phase composition due to the chemical attack. The phase identification by SEM-EDX is based on an average chemical composition, but compared with the results by SyXRD leads to satisfactory results. However, for a more detailed view, especially into the interaction of crystalline phases, a high resolution X-ray diffraction method based on synchrotron radiation furnishes more precise spatial results.

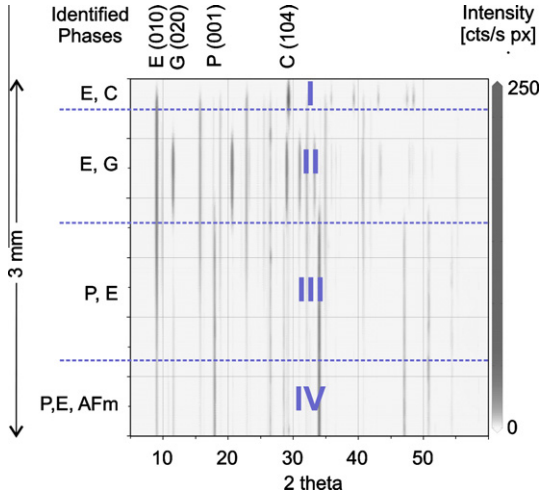


**Fig. 4.** Diffraction pattern in a top view collected from the surface (top) down to profile depth of 3 mm. The identified phases within the four different zones (I–IV) are ettringite (E), gypsum (G), portlandite (P) and an AFm solid solution (AFm).

## 6. Conclusion

The study performed by μXRF allows localizing the secondary phases and leads to a more efficient analysis by SEM-EDX and SyXRD focused on the crucial change of the phase composition. Elemental mappings are often mentioned as an experimental procedure analyzing the degradation of cement or the cement matrix of cementitious materials. The advantages combining it with SEM-EDX and SyXRD analysis are presented in this study. The SEM-EDX provided valuable information on the change of the phase composition due to the sulfate attack. Several secondary phases were identified by calculating the Al/Ca and S/Ca atom ratios and visualizing the data. In this way, the interaction of the sulfate solution with the cementitious material can be characterized by using an experimental setup on the laboratory scale. For a more detailed view, a high resolution X-ray diffraction method based on synchrotron radiation is essential.

## Acknowledgments

M. C. Schlegel thanks the BAM Federal Institute for Materials Research and Testing, Berlin, Germany, for a grant within its Ph. D. program. We thank Andre Gardei and Simone Rolf for technical support and Jan Erik Linqvist from the CBI Swedish Cement and Concrete Research Institute, Borås, Sweden, for supporting the SEM-EDX analysis.

## References

[1] Bensted J. Thaumasite-direct, woodfordite and other possible formation routes. Cem Concr Compos 2003;25:873–7.
[2] Churakov SV. Structure of the interlayer in normal 11 angstrom tobermorite from an ab initio study. Eur J Mineral 2009;21:261–71.
[3] Dobson DP, Alfredson M, Holzapfel C, Brodholt JP. Grain-boundary enrichment of iron on magnesium silicate perovskite. Eur J Mineral 2007;19:617–22.
[4] Schlegel MC, Mueller U, Panne U, Emmerling F. Deciphering the sulfate attack of cementitious materials by high-resolution micro-X-ray diffraction. Anal Chem 2011;83:3744–9.
[5] Famy C, Brough AR, Taylor HFW. The C–S–H gel of Portland cement mortars. Part I. The interpretation of energy-dispersive X-ray microanalyses from scanning electron microscopy, with some observations on C–S–H, AFm and AFt phase compositions. Cem Concr Res 2003;33:1389–98.
[6] Famy C, Scrivener KL, Crumbie AK. What causes differences of C–S–H gel grey levels in backscattered electron images? Cem Concr Res 2002;32:1465–71.
[7] Francois M, Renaudin G, Evrard O. A cementitious compound with composition 3CaO.Al2O3.CaCO3.11H(2)O. Acta Crystallogr, C 1998;54:1214–7.
[8] Giorgetti G, Baroni C. High-resolution analysis of silica and sulphate-rich rock varnishes from Victoria Land (Antarctica). Eur J Mineral 2007;19:381–9.
[9] Glasser FP, Kindness A, Stronach SA. Stability and solubility relationships in AFm phases. Part 1. Chloride, sulfate and hydroxide. Cem Concr Res 1999;29:861–6.
[10] Goetz-Neunhoeffer F, Neubauer J. Refined ettringite $Ca_6Al_2(SO_4)_{(3)}(OH)_{(12)}$ center dot $26H_{(2)}O$ structure for quantitative X-ray diffraction analysis. Powder Diffr 2006;21:4–11.
[11] Gollop RS, Taylor HFW. Microstructural and microanalytical studies of sulfate attack .1 Ordinary Portland-cement paste. Cem Concr Res 1992;22:1027–38.

[12] Konrad-Schmolke M, O'Brien PJ, Heidelbach F. Compositional re-equilibration of garnet: the importance of sub-grain boundaries. Eur J Mineral 2007;19:431–8.
[13] Kuzel HJ, Baier H. Hydration of calcium aluminate cements in the presence of calcium carbonate. Eur J Mineral 1996;8:129–41.
[14] Liebl C, Kuntcheva B, Kruhl JH, Kunze K. Crystallographic orientations of quartz grain-boundary segments formed during dynamic recrystallization and subsequent annealing. Eur J Mineral 2007;19:735–44.
[15] Matschei T, Lothenbach B, Glasser FP. The AFm phase in Portland cement. Cem Concr Res 2007;37:118–30.
[16] Melzer S, Gottschalk M, Andrut M, Heinrich W. Crystal chemistry of K-richterite-richterite-tremolite solid solutions: a SEM, EMP, XRD, HRTEM and IR study. Eur J Mineral 2000;12:273–91.
[17] Mesbah A, Rapin JP, François M, Cau-dit-Coumes C, Frizon F, Leroux F, et al. Crystal structures and phase transition of cementitious bi-anionic AFm-($Cl^-$, $CO_3^{2-}$) compounds. J Am Ceram Soc 2011;20:261–8.
[18] Naik NN, Jupe AC, Stock SR, Wilkinson AP, Lee PL, Kurtis KE. Sulfate attack monitored by microCT and EDXRD: influence of cement type, water-to-cement ratio, and aggregate. Cem Concr Res 2006;36:144–59.
[19] Paris O, Li CH, Siegel S, Weseloh G, Emmerling F, Riesemeier H, et al. A new experimental station for simultaneous X-ray microbeam scanning for small- and wide-angle scattering and fluorescence at BESSY II. J Appl Crystallogr 2007;40:466–70.
[20] Richardson IG, Groves GW. Microstructure and microanalysis of hardened ordinary Portland-cement pastes. J Mater Sci 1993;28:265–77.
[21] Richardson IG. The nature of C–S–H in hardened cements. Cem Concr Res 1999;29:1131–47.
[22] Rumori C, Mellini M, Viti C. Oriented, non-topotactic olivine → serpentine replacement in mesh-textured, serpentinized peridotites. Eur J Mineral 2004;16:731–41.
[23] Schimrosczyk A, Koepke J, Schmidt-Dohl F. Trace element analysis of belite in hardened cement bonded materials using electron microprobe analysis. Eur J Mineral 2007;19:105–12.
[24] Scrivener KL. Backscattered electron imaging of cementitious microstructures: understanding and quantification. Cem Concr Res 2004;26:935–45.